W. Böhme and W. Schmitt**

On the Ductile Crack Initiation and Propagation Behaviour of a Pressure Vessel Steel under Impact Loading

REFERENCE Böhme, W. and Schmitt, W., **On the ductile crack initiation and propagation behaviour of a pressure vessel steel under impact loading**, *Defect Assessment in Components – Fundamentals and Applications*, ESIS/EGF9 (Edited by J. G. Blauel and K.-H. Schwalbe) 1991, Mechanical Engineering Publications, London, pp. 681–692.

ABSTRACT For the determination of dynamic J resistance curves, drop weight experiments were performed with large three-point bend specimens made from a ferritic pressure vessel steel. The specimens were side-grooved and fatigue-pre-cracked. Different amounts of ductile crack extension up to 25 mm were achieved by varying the available impact energy. The experiments were analysed with different experimental techniques including optical methods with high-speed photography. Mainly the measured hammer load signals were used to calculate J integral values. Together with the measured crack extensions dynamic J resistance curves were determined. The results are significantly above respective static or published dynamic data. At a crack extension of about 3 mm there is a significant change in the slope. Examinations of the fracture surface and metallographic sectioning perpendicular to the crack front showed that behind the stretched zone the ductile main crack is accompanied by a side crack up to 3 mm long. Its size correlates approximately with that crack length where the slope of the J resistance curve is changing. The additional energy needed for the formation of side cracks might explain the high J integral values at a given size of the main crack. For comparison, further experiments were examined in a similar manner. The results indicate that with increasing loading rate and specimen size the tendency to develop side cracks increases in correlation with higher resistance curves. Finally, an attempt is made to discuss the relevance of this effect for the behaviour of components.

Introduction

Dynamic fracture resistance curves were determined by impact tests in order to quantify the rate dependence of the toughness properties at initiation and fast crack propagation for a ductile material. With impact velocities of several metres per second the achieved loading rates were five to six orders of magnitude above usual static rates, and can be considered as an upper limit for loading rates expected during postulated emergency and faulted conditions in a pressurised water reactor.

The investigations were performed with the ferritic pressure vessel steel 22 NiMoCr 3 7 ($\triangleq$ ASTM A 508 Cl 2) at temperatures in the upper shelf regime of the Charpy energy of about 200 Joule. The evaluations are focused on the processes during ductile crack initiation and extension. The results are summarised here, whereas more details are given in **(1)**.

* Fraunhofer-Institut für Werkstoffmechanik, Wöhlerstrasse 11, D-7800 Freiburg, FRG.

Experiments

From a heat of the steel 22 NiMoCr 3 7 (≙ ASTM A 508 Cl 2) relatively large bend specimens (SENB 90) with dimensions 495 mm × 90 mm × 45 mm were machined in *L–S* orientation. The in-plane dimensions are 9 times, the thickness is 4.5 times larger than for ISO V or Charpy specimens. The specimens were fatigued and side-grooved (20 percent). The initial crack lengths a_0 were 45.6 ± 1.4 mm. The SENB 90 specimens were loaded in three-point bending with a support distance $S = 4W = 360$ mm in a drop-weight tower (see Fig. 1). The impact velocity was 6.77 m/s. The impact energy was varied by using different masses of the hammer in the range of 111–282 kg; thus, different amounts of ductile crack extension could be achieved in different tests.

From parts of a broken specimen without plastic deformations Charpy specimens (SENB 10) were machined and provided with fatigue cracks and side-grooves like the SENB 90 specimens. The initial crack lengths were a_0 = 5.5 ± 0.3 mm. The Charpy specimens were loaded in a pendulum with a mass of the hammer of 20 kg. Different amounts of ductile crack extension were achieved by a variation of the impact velocities between 0.55 m/s and 1.73 m/s.

In all experiments the load P was measured at the top of the impacting hammer by means of statically calibrated strain gauges and recorded as a

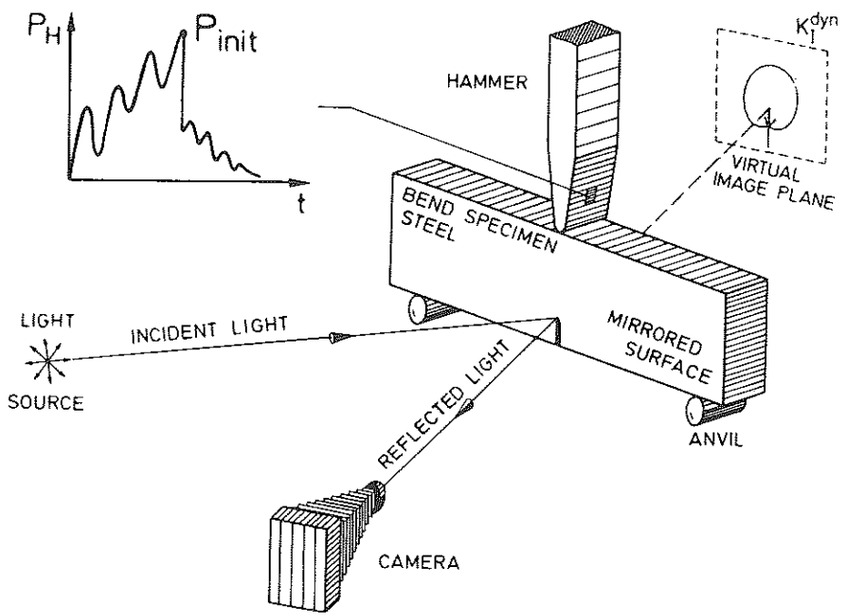

Fig 1 Experimental set-up (schematic)

function of the time *t*. The load signal was integrated twice according to references **(2)(3)** yielding the time-dependent displacement of the hammer, *s*(*t*), and thus load–displacement records *P*(*s*) were constructed. Characteristic examples are given in Fig. 2 for the SENB 90 specimens and in Fig. 3 for the Charpy specimens.

Large oscillations occur at the very beginning of the load signal with the first peak being the so-called inertia peak. These oscillations are caused by elastic wave propagation and vibration effects and are discussed elsewhere **(4)–(6)** in more detail. Because of the damping effect of plastic deformation especially near the impact position these oscillations level out early. Therefore, the quasi-static evaluation performed here leads to reasonable accuracy after about three oscillations.

In the experiments with SENB 90 specimens further measurements were performed simultaneously. Almost all specimens were instrumented by strain gauges in order to get some information about the actual loading in the specimen in addition to the external load record. Despite of the oscillating external load in the very beginning of the impact event the strain gauge signals show an almost linear increase of the crack tip loading in agreement with predictions for this type of specimen **(5)–(8)**. From the slope of the elastic strain gauge response the initial crack tip loading rates dK/dt are determined to be about $7 \cdot 10^5$ MPa$\sqrt{\text{m}}$/s for the SENB 90 tests (fixed impact velocity) and

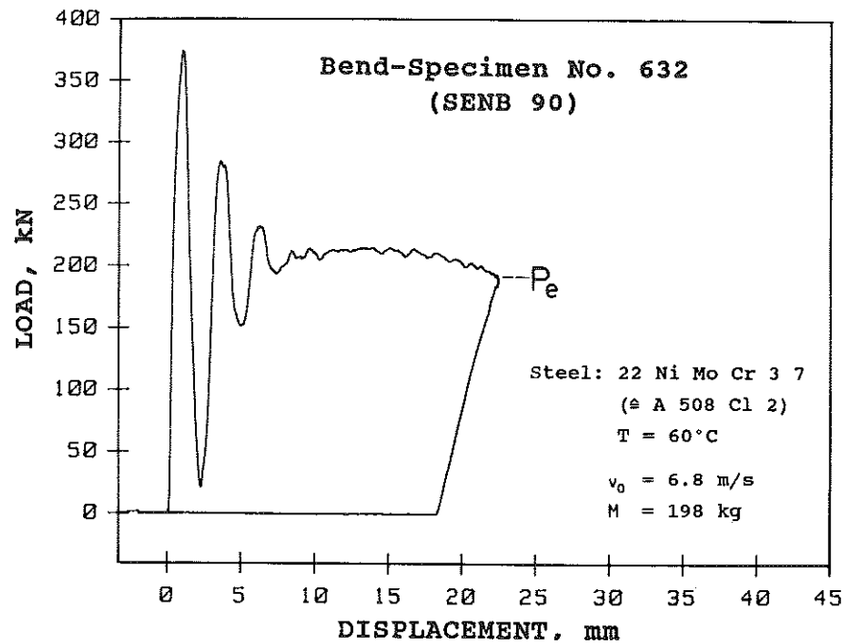

Fig 2 Load–displacement diagram *P*(*s*) for a SENB 90 specimen

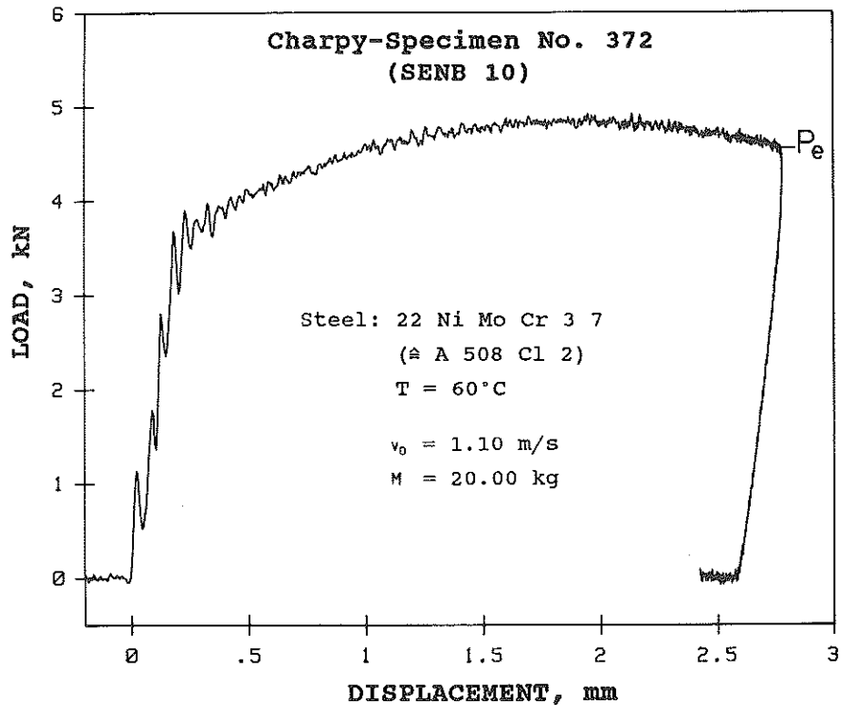

Fig 3 Load–displacement diagram $P(s)$ for a Charpy specimen

between 1.4×10^5 MPa$\sqrt{\text{m/s}}$ and 3.2×10^5 MPa$\sqrt{\text{m/s}}$ for the SENB 10 tests depending on the impact velocity. These loading rates differ only by a factor of two to five and, therefore, can be considered as of the same order of magnitude, whereas usual static loading rates are about five decades lower.

For a direct determination of the crack tip loading the shadow-optical method of caustics was applied in reflection; to this end the surfaces of some of the specimens had to be lapped and polished. The caustics were recorded with a 24-spark high speed camera during the tests. As an example, Fig. 4 shows a series of such caustics. Caused by the very high J integral values obtained here the caustic pattern in front of the crack is interfering with a shadow pattern formed at the point of impact. A quantitative evaluation of J values based on the diameter of the caustics is in progress.

Additionally in some cases the deformation pattern of the specimen surface was determined directly by high speed photography of the specimen surface where a grid was applied by scratching. From these pictures the global bending displacement of the specimen and the opening of the crack flanks may be determined.

The experiments were carried out at temperatures in the upper shelf of the Charpy energy (200 J) mainly at 60°C. A few SENB 90 specimens were also

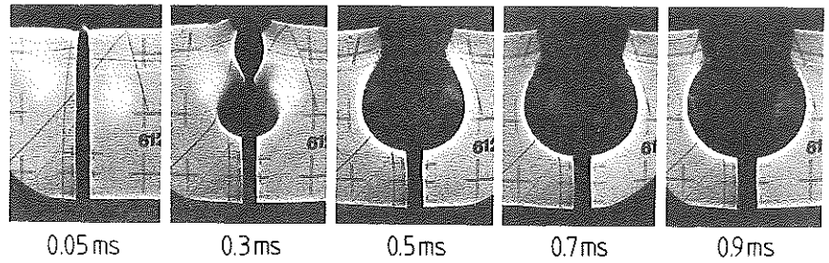

Fig 4 Series of caustics obtained during impact of a bend specimen at very high J-integral values

tested at room temperature and at 90°C. In some experiments at 60°C a sudden change of the fracture mode into cleavage could be observed even after several millimetres of ductile crack extension **(1)**. In the following, only the phase of ductile crack extension will be explored and evaluated. The results do not show a significant influence of the test temperature on the amount of ductile tearing so that the J integral values and resistance curves will be discussed independent of the temperature.

Results

It was the first goal of the investigations to determine a J resistance curve for dynamic loading. Since for impact loading no standard evaluation scheme is available a procedure in accordance with ASTM E 813 **(9)** and ASTM E 1152 **(10)** (multi-specimen technique) was chosen. Here, the J integral values are determined from the load displacement record $P(s)$ and correlated with the respective amounts of ductile crack propagation Δa determined after the test by optical inspection of the fracture surfaces.

Figure 5 shows dynamic J values versus the respective amounts of ductile crack extension for the SENB 90 and Charpy specimens. The linear shape of the J–R curve for the SENB 90 specimens above $\Delta a \approx 3$ mm is confirmed through further data points up to $\Delta a \approx 16$ mm (see **(1)**). The J–R curve for the Charpy specimens results from 10 data points with only little scatter (see **(1)**). In addition the calculated blunting line $J = 2\sigma_y \Delta a$ is given. Since the dynamic stress strain curve of the material was not available a dynamic yield stress of $\sigma_y^{dyn} = 700$ MPa was chosen which is 25 percent above the statically determined yield stress $\sigma_y^{stat} = 560$ MPa.

The Charpy data yield J values up to about 1 MN/m, while the results from the SENB 90 specimens are significantly higher. The J values exceed the maximum J capacity J_{max} of the specimens as proposed in the standard after only very small amounts of crack extension (Charpy specimen: $J_{max} = 0.35$ MN/m, SENB 90 specimen: $J_{max} = 1.58$ MN/m). Since better evaluation methods are not yet available the further discussion of the results will also be done on the basis of the J integral concept.

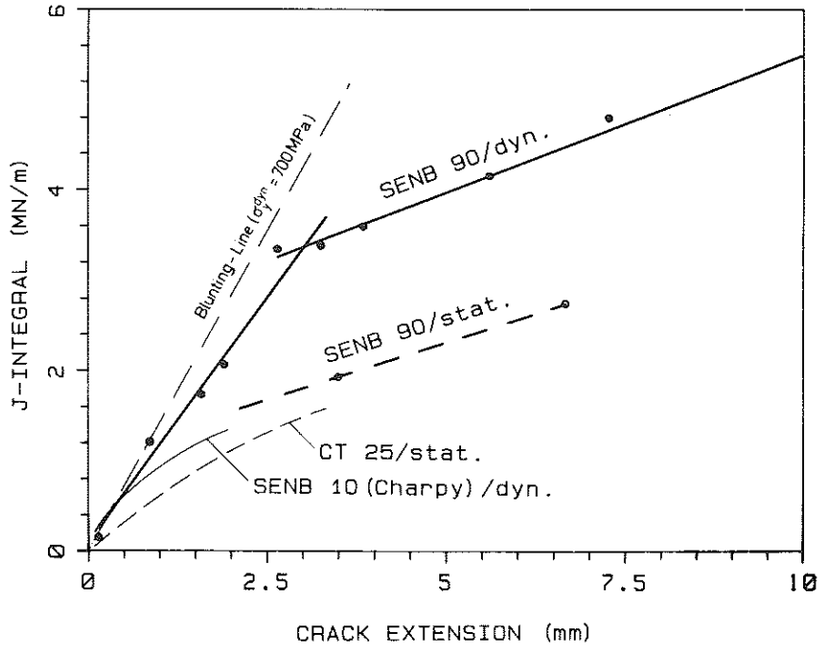

Fig 5 Static and dynamic *J–R* curves for specimens of different type and size (22 NiMoCr 3 7 ≙ A 508 Cl 2)

The Charpy data are well in agreement with comparable results for A 533 B and A 508 steels reported by Curr *et al.* **(11)** or Kobayashi *et al.* **(12)**. At first glance the SENB 90 data seem to follow the blunting line up to about $\Delta a \approx 3$ mm, although the so-called stretched zone ends as early as $\Delta a \approx 0.1$ mm, indicating a significant amount of ductile crack propagation for all data points reported. Only at very high J values of about 3.3 MN/m the slope of the curve changes remarkably leading to a less steep increase of the resistance curve, however at very high J values.

For comparison, Fig. 5 shows further results of the same heat from static tests with SENB 90 specimens **(13)** and with CT-25 specimens **(14)**. Two results from static SENB 90 tests define a slope which nicely matches the slope of the dynamic curve for the SENB 90 specimens for large crack extensions. This points to the fact that the tearing modulus or the crack propagation energy will not be significantly different between static and dynamic loading.

The absolute values of the static curve lie significantly below those from the dynamic curve, however. This is apparently caused by the fact that for static loading the transition from the steeper to the flatter part of the curve occurs at smaller amounts of crack extension than for dynamic loading. The static curve intersects with the blunting line at a crack extension of about 1 mm as opposed to about 3 mm for the impact tests (see also next section). The static

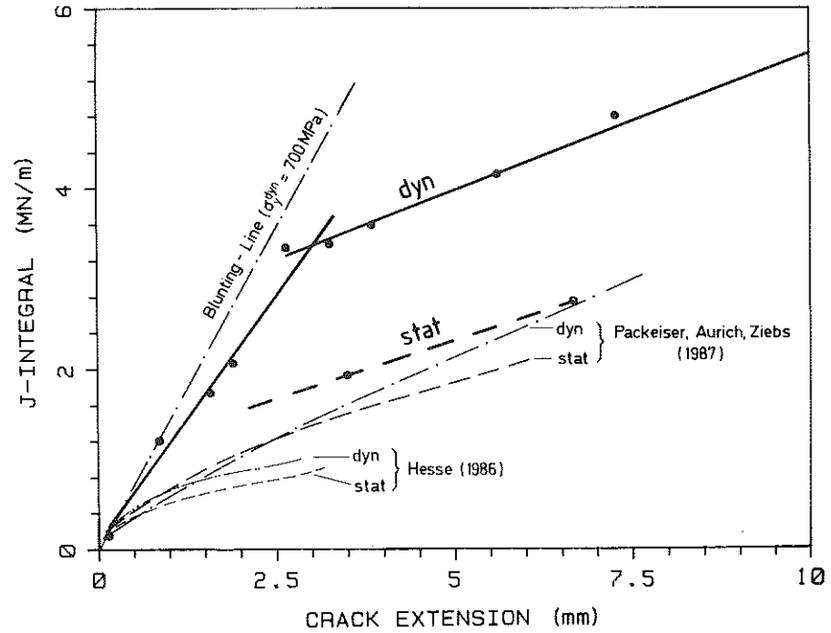

Fig 6 Static and dynamic *J–R* curves in comparison to data from literature

J–R curve from the CT-25 compact specimens forms the lower bound to all other curves.

For a further comparison, Fig. 6 compiles static and dynamic resistance curves for similar pressure vessel materials **(15)(16)**. These are also significantly below the SENB 90 results reported here. The differences are explained in **(1)** based on analyses of the fracture surfaces described below. Numerical simulations **(17)** conducted in parallel to the experiments also yielded resistance curves only slightly below those determined directly from the experiments and therefore confirm the results and conclusions reported here.

Fracture analysis

Examination of the fracture surfaces by scanning electron microscopy revealed no indications for a change of the ductile fracture mode after a crack extension of about 3 mm which could explain the sudden drop in the slope of the resistance curve. Only at $\Delta a \approx 0.3$ mm a crevice was found running parallel to the crack front which is partly interrupted or displaced. This crevice indicates side cracks going into the depth of the material. Therefore, additional metallographic sectionings were performed perpendicular to the crack front at those positions where the crevice was most remarkable. In Fig. 7 one sees for a dynamically loaded SENB 90 specimen that behind the crevice there is a side crack of about 3 mm hiding below the ductile main crack.

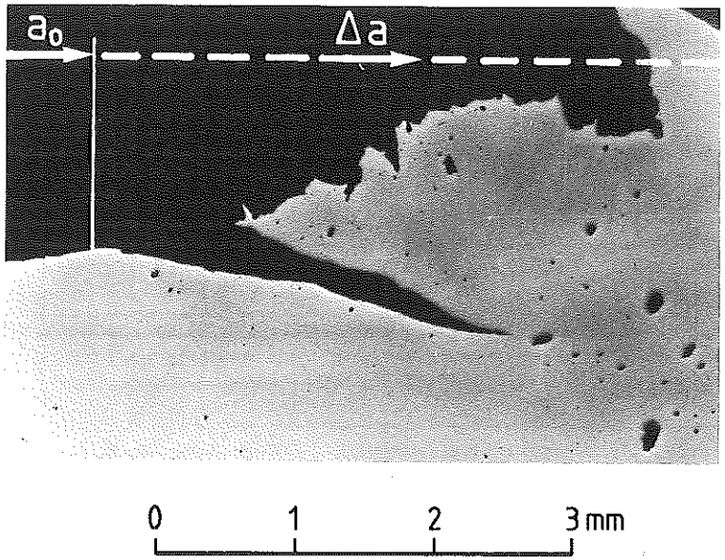

Fig 7 Polished section of a dynamically loaded SENB 90 specimen

This leads to the conclusion that in the beginning of the fracture process after crack tip blunting at least two cracks were formed and extended. It might be expected that these two cracks consume more energy for propagation than a single crack, since, e.g., for a given displacement the crack tip opening for either of two (or more) nearby cracks will be lower than for a single one. This would qualitatively explain the initially steeper J–R curve if multiple cracks are present, and the subsequent smaller slope of the curve if only a single main crack is propagating. In addition, the lengths of the obtained side cracks agree well with the amount of crack extension where the change of slope occurs in the resistance curve.

It is worth noting, that this side crack formation and the corresponding steep J–R curve occurs within the ASTM limits, where the data are close to the calculated blunting line. The propagation of a single crack, however could only be obtained beyond the ASTM validity range.

It is furthermore remarkable that the main crack has a ductile fracture surface with dimples while the side crack appears smooth (see Fig. 7), which might be an indication for shear failure along slip lines. Thus, ductile crack initiation is accompanied here by macroscopic side cracks which can obviously be formed at slip lines ± 45 degrees off the main crack. Therefore, two- or even three-crack systems are conceivable about initiation. Although a complete explanation of this mechanism is not yet possible the principal influence of loading rate and specimen size on this effect may be deduced at least quali-

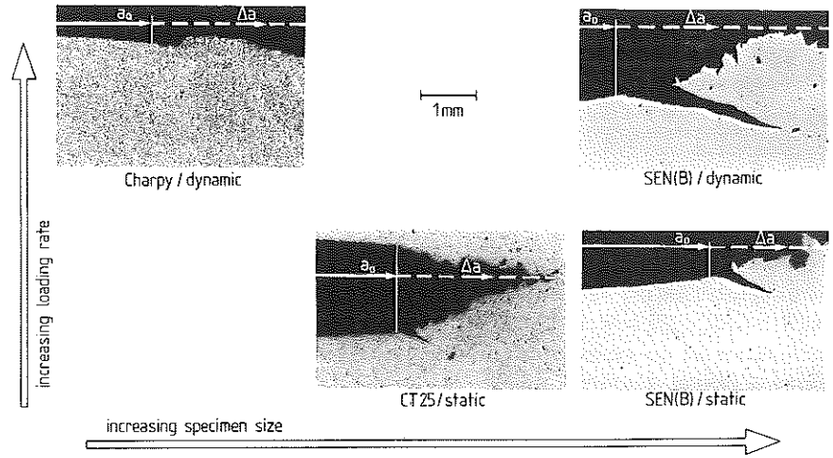

Fig 8 Polished sections of the crack initiation region for different specimen and loading rates

tatively in Fig. 8, and, in addition, the consequences with respect to the crack resistance behaviour can be discussed (see (1)).

With increasing loading rate, and in particular with increasing specimen size the tendency to form side cracks increases. At the same time higher resistance curves with a significant change in slope are observed. This change occurs at amounts of crack extension which are in agreement with the size of the side cracks.

Discussion

Following the current understanding of ductile crack initiation and propagation the first phase is characterised by crack tip blunting and the formation of a stretched zone. In the following second phase a single ductile crack extends. Transition from phase 1 to phase 2 should be accompanied by a significant change in slope of the J–R curve defining a critical initation value J_i.

This simple model has to be extended now in the light of the previously discussed results as sketched schematically in Fig. 9. Phase I corresponds to the former phase 1 and is related to the process of crack tip blunting. It is, however, now followed by a new phase II, where one propagating main crack is accompanied by additional side cracks. Only in phase III (corresponding to the former phase 2) the crack propagation of a single ductile main crack takes place.

The three phases, I–III, correspond to three different slopes of the resistance curve defining two kinks with two different critical J values. J_i corresponds to the well known initiation value. The new value J_i^{RL} is a critical value for the start of the ductile extension of a single crack.

This fracture resistance value J_i^{RL} could be a material parameter which, however, depends strongly on the loading conditions. The results presented

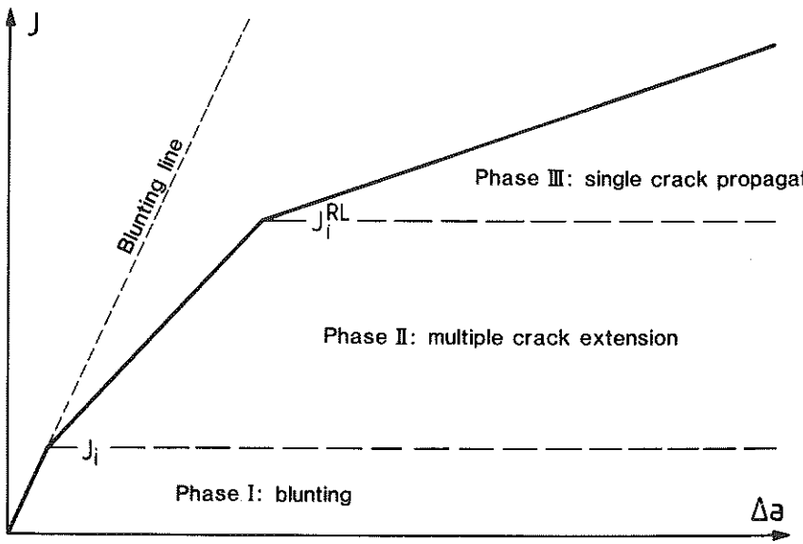

Fig 9 Modified *J–R* curve (schematic)

here indicate that J_i^{RL} is lowest at low loading rates and for small specimens. Therefore, it seems to be reasonable to use statically loaded small specimens, e.g., compact specimens if lower bound ductile fracture resistance curves are to be determined. The value of J_i^{RL} then obviously will be so close to J_i that both kinks may no longer be distinguished resulting in lower bound *J–R* curves with a continuously changing slope.

On the other hand J_i^{RL} obviously increases with loading rate and especially with specimen size. Presumably the kink in the resistance curve could be resolved for the first time so clearly in this investigation because two effects each of which promoting phase II and high values of J_i^{RL} were combined: First, relatively large specimens were utilised and, secondly, the tests were performed at high loading rates. It might be possible that the high toughness level of this material, as indicated by the CT 25 data, contributes to this effect as well.

Of particular interest for the evaluation of components is the fact that J_i^{RL} increases with increasing specimen size. Therefore, phase II with the corresponding steeper resistance curve could be important for larger components. If the trends reported here could be confirmed, additional safety margins may be expected for components.

Conclusions

The investigations aimed at the characterisation of the ductile fracture of a pressure vessel steel at elevated loading rates are based on the *J* integral concept. To this end, impact experiments were performed with SENB 90 specimens in a drop weight tower and with Charpy specimens in a pendulum. All specimens were fatigued and sidegrooved.

From the measured hammer load signals *J* integral values were determined. By a multi-specimen technique the available impact energy was varied to achieve different amounts of crack extension and thus dynamic *J–R* curves were determined. the *J–R* curve of the SENB 90 specimens lies significantly above related static and dynamic results. Also, a significant change in slope was found at $\Delta a \approx 3$ mm.

Investigations of the fracture surfaces and sectionings perpendicular to the fracture surface revealed that the stretched zone is followed by a region where the ductile main crack may be accompanied by side cracks up to about 3 mm length. This length corresponds approximately to the crack length at which the *J–R* curve exhibits a change in slope. A peer investigation of other experiments gives indications that the tendency to develop side cracks and therefore to increase the fracture resistance curve increases with the loading rate and in particular with the specimen size.

Acknowledgements

The authors are grateful to the Bundesminister für Forschung und Technologie (BMFT) who supported this work under the contract number 1500488. They also thank Mr M. Hug for thoroughly performing the experiments.

References

(1) BÖHME, W. (1989) Experimentelle Untersuchungen zum elastisch–plastischen Bruchverhalten eines Druckbehälterstahls unter dynamischer Beanspruchung, Scientific report W 3/89, Fraunhofer-Institut für Werkstoffmechanik (IWM), Freiburg.
(2) *DVM-Merkblatt 001* (1986) Meßtechnische Anforderungen beim instrumentierten Kerbschlagbiegeversuch.
(3) *Stahl–Eisen–Prüfblatt* 1315 (1987) Kerbschlagbiegeversuch mit Ermittelung von Kraft und Weg.
(4) KALTHOFF, J. F., BÖHME, W., WINKLER, S., and KLEMM, W. (1981) Measurements of dynamic stress intensity factors in impacted bend specimens, CSNI Specialists Meeting on Instrumented Precracked Charpy Testing, Electric Power Research Institute (EPRI), in *EPRI NP-2102-LD*, pp. 1–17.
(5) BÖHME, W. and KALTHOFF, J. F. (1982) The behavior of notched bend specimens in impact testing, *Int. J. Fracture*, **20**, R139–R143.
(6) BÖHME, W. (1985) Experimentelle Untersuchungen dynamischer Effekte beim Kerbschlagbiegeversuch, Scientific report W 1/85, IWM, Freiburg.
(7) BÖHME, W. (1990) Dynamic key-curves for brittle fracture impact tests and establishment of a transition time, 21st National Symposium on Fracture Mechanics, Annapolis, MD, USA, *ASTM STP 1074* pp. 144–156.
(8) BÖHME, W. and KALTHOFF, J. F. (1985) On the quantification of dynamic effects in impact loading and the practical application for K_{Id}-determination, *J. Phys., Coll., C5, Suppl.* No 8, **46**, 213–218.
(9) ASTM E 813–87 (1987) *Annual Book of ASTM Standards*, ASTM, Philadelphia, Vol. 03.01.
(10) ASTM E 1152–87 (1987) *Annual Book of ASTM Standards*, ASTM, Philadelphia, Vol. 03.01.
(11) CURR, M. R., MACGILLIVRAY, H. J. and TURNER, C. E. (1986) Dynamic Fracture Mechanics, IMechE Seminar, London.

(12) KOBAYASHI, T., YAMAMOTO, I. and NIIOMI, M. (1986) *Engng Fracture Mech.*, **24**, 773–782.
(13) VOSS, B. and FALK, L. (1988) Bestimmung statischer *J–R* Kurven mit Biegeproben eines Druckbehälterstahles, unpublished results and private communication, IWM, Freiburg.
(14) SUN, D. and VOSS, B. (1988) Bestimmung statischer *J–R* Kurven mit CT-25 Proben eines Druckbehälterstahles, unpublished results and private communication, IWM, Freiburg.
(15) HESSE, W. (1986) *Zur Auswirkung hoher Beanspruchungsgeschwindigkeiten auf das Versagensverhalten von Baustählen unter einsinniger Zugbeanspruchung*, Dissertation, RWTH Aachen.
(16) PACKEISER, R., AURICH, D., and ZIEBS, J. (1987) Influence of loading rate on the crack resistance curve and the initiation temperature, *Nucl. Engng Des.*, **102**, 487–493.
(17) VO, T. and STÖCKL, H. (1989) Simultationen von Schlagversuchen an großen Biegeproben aus einem Druckbehälterstahl mit der Methode der finiten Element, Scientific report, W 2/89, IWM, Freiburg.